ELSEVIER

Earth and Planetary Science Letters 160 (1998) 763–776

EPSL

Bubble growth in highly viscous melts: theory, experiments, and autoexplosivity of dome lavas

Oded Navon *, Anatoly Chekhmir, Vladimir Lyakhovsky

Institute of Earth Sciences, The Hebrew University, Jerusalem 91904, Israel

Received 31 October 1997; revised version received 4 June 1998; accepted 6 June 1998

Abstract

We examine the physics of growth of water bubbles in highly viscous melts. During the initial stages, diffusive mass transfer of water into the bubble keeps the internal pressure in the bubbles close to the initial pressure at nucleation. Growth is controlled by melt viscosity and supersaturation pressure and radial growth under constant pressure is approximately exponential. At later stages, internal pressure falls, radial growth decelerates and follows the square-root of time. At this stage it is controlled by diffusion. The time of transition between the two stages is controlled by the decompression, melt viscosity and the Peclet number of the system. The model closely fit experimental data of bubble growth in viscous melts with low water content. Close fit is also obtained for new experiments at high supersaturation, high Peclet numbers, and high, variable viscosity. Near surface, degassed, silicic melts are viscous enough, so that viscosity-controlled growth may last for very long times. Using the model, we demonstrate that bubbles which nucleate shortly before fragmentation cannot grow fast enough to be important during fragmentation. We suggest that tiny bubbles observed in melt pockets between large bubbles in pumice represent a second nucleation event shortly before or after fragmentation. The presence of such bubbles is an indicator of the conditions at fragmentation. The water content of lavas extruded at lava domes is a key factor in their evolution. Melts of low water content ($<$0.2 wt%) are too viscid and bubbles nucleated in them will not grow to an appreciable size. Bubbles may grow in melts with $\sim$0.4 wt% water. The internal pressure in such bubbles may be preserved for days and the energy stored in the bubbles may be important during the disintegration of dome rocks and the formation of pyroclastic flows.

Keywords: vesicular texture; experimental studies; numerical models; shield volcanoes; pumice

1. Introduction

The volcanic eruptions associated with formation of lava domes in Mount St. Helens, Mount Unzen, and recently the Soufriere Hills in Montserrat focused attention on the evolution of highly viscous melts and the hazards associated with them [2–5]. Attention has also been devoted to the auto-explosivity of lava during dome collapse and its role in initiating pyroclastic flows [6,7]. The exsolution of water and the growth of bubbles may play an important role in the build-up of stresses in such magmas [8]. Following extensive effort in modelling bubble growth in viscous magmas [9–16], Lyakhovsky et al. [17] presented the first experimental verification of a growth model. The good agreement between measured bubble sizes and model calculations validated

* Corresponding author. Tel: +972-2-658-6513; Fax: +972-2-566-2581; E-mail: oded@vms.huji.ac.il

0012-821X/98/$19.00
PII S0012-821X(98)00126-5

the role of water diffusion during growth. However, the experimental conditions did not allow testing of the effect of viscosity on the growth rate.

The viscosity of rhyolitic melts with ~5 wt% water at 800–850ºC is less than 10^5 Pa s [18]. Such viscosities may affect the growth of a bubble only during a fraction of the first second (see below). Much higher viscosities, of the order of 10^7 Pa s or higher are required in order to observe experimentally the role of viscous deformation of the melt around a growing bubble. Such high viscosities are reached at 800–850ºC in degassed melts with water content of less than 1 wt%, or in melts with 3–5 wt% water at much lower temperatures [18,19].

Recently, Bagdassarov et al. [1] examined the growth of bubbles in rhyolite with 0.14 wt% water. Here we re-interpret their results and use them to test the growth model at high viscosities. We also present new experimental results on vesiculation in rhyolite with 5 wt% water at low temperatures. The extreme degassing from 5 to less than 0.2 wt% water allowed us to test the model under conditions where variation in viscosity in the vicinity of the bubble is important. Although the experiments were carried out under constant pressure, the experimentally verified model may be safely extended to simulate bubble growth under conditions where in addition to variable viscosity and diffusion coefficient, pressure may also be varied. Here, we apply the model to examine vesiculation in fragments of pumice and to estimate the energy stored in cooling lava domes. In these two cases, the ambient pressure is close to atmospheric and is assumed to be constant.

2. The physics of bubble growth in viscous melts

The process of bubble growth begins with the formation of nuclei in a supersaturated melt. According to classical nucleation theory, the critical nucleus is in unstable chemical and mechanical equilibrium with the melt. Gas pressure within the nucleus relates to the melt supersaturation through the Henry constant and is compensated by the ambient pressure and Laplace surface tension (see [20] for a recent review). For nuclei with radius $R_0 > R_{CR}$ there exists a net outward force on the interface and the bubble grows. As the tiny bubble expands, gas pressure (P_g) decreases and water molecules evaporate from the interface in order to re-establish equilibrium. This lowers the concentration at the interface (C_R) relative to the melt far away from the bubble (C_0) and leads to diffusive mass flux of water towards and into the growing bubble. The water influx keeps P_g close to its initial value in the small bubble while the force due to surface tension decreases. This ensures continued growth of the bubble.

In viscous melts, growth is limited by the high melt viscosity and the two processes, water diffusion and viscous deformation control the evolution of the bubble. The ratio between the time scale for diffusion, $\tau_d = R^2/D$, and for viscous deformation, $\tau_v = \eta/\Delta P$, is the non-dimensional Peclet number:

$$Pe = \frac{\tau_d}{\tau_v} = \frac{\Delta P R^2}{\eta D}. \quad (1)$$

When $Pe \gg 1$, diffusive mass transfer is unimportant relative to the rate of expansion. Such conditions may evolve during fast ascent of magmas, where ΔP does not vanish and R grows. During slow ascent or in lava domes, Pe is of the order 1 or smaller and diffusive mass transfer is the main motive for growth.

Three stages may be defined during bubble growth under constant pressure. In the first, diffusion into the small bubble is very efficient and succeeds in keeping the internal pressure close to its initial value. At this stage, growth is limited by the viscous resistance of the melt. In the second stage the pressure in the bubble is maintained at slightly above the ambient pressure and growth is limited by diffusion. Finally, in a multi-bubble situation, all excess water is taken by the bubbles, which asymptotically approach their final radius. Growth during the second and third stages was tested experimentally by Lyakhovsky et al. [17]. In this paper, we examine the first stage of growth and the transition between the first and second stages (Fig. 1). We begin with the general mathematical formulation of the model and asymptotic solutions that describe the growth process for each stage separately. Then we compare these solutions with numerical simulations based on full formulation, and test them against experimental data.

In cases where the Peclet number is smaller than one, the diffusion is fast enough to establish a steady-state concentration profile. This enables a significant

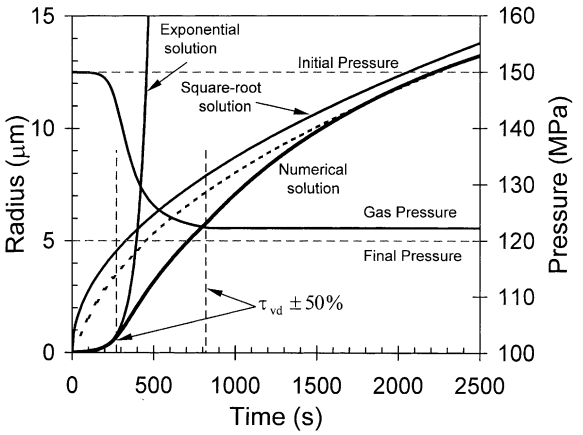

Fig. 1. Bubble growth at constant final pressure. At the initial stages the numerical simulation (thick solid line) closely follows the exponential solution (Eq. 4), later it approaches the square root solutions. The dashed line denotes the solution with both terms of (Eq. 7), the solid line represent the first term only. The internal pressure in the bubble remains close to its initial value during the first stage and then quickly falls to slightly above the final pressure. Also shown is the time of transition between the exponential and the square-root solutions, τ_{vd}. The two thin vertical dashed lines correspond to 0.5 and 1.5 of the approximation for τ_{vd} (Eq. 11). $P_0 = 150$ MPa, $P_f = 120$ MPa, $\eta = 5 \times 10^8$ Pa s, $D = 10^{-12}$ m^2/s, $C_0 = 5.5$ wt%.

simplification of the mathematical procedure [17] and allows derivation of asymptotic analytical solutions for various stages of growth. Most important, the concentration gradient at the interface between a growing bubble and supersaturated melt may be expressed analytically [17]. For a solitary bubble we obtain:

$$\left(\frac{\partial C}{\partial r}\right)_R = \frac{C_0 - C_R}{R} = \frac{C_0 - K_H\sqrt{P_g}}{R}, \tag{2}$$

where Henry's law for water is approximated by a square-root dependence [21]. The solution of the Navier–Stokes equation for a solitary, non-interacting bubble growing under constant ambient pressure in an isoviscous melt is reduced to:

$$\Delta P \equiv P_g - P_f = \frac{2\sigma}{R} + 4\eta\frac{v_R}{R}. \tag{3}$$

In small bubbles, where the surface/volume ratio is high, diffusion is very efficient and succeeds in keeping P_g close to its initial value. Under these approximations radial growth follows an exponential law:

$$R = R_{CR} + (R_0 - R_{CR})\exp\left(\frac{\Delta P}{4\eta}t\right). \tag{4}$$

If $R_0 \gg R_{CR}$, this expression converges with the simpler expression given by Toramaru [10]. However, for a nucleating bubble R_0 is just slightly larger than R_{CR}, and the pre-exponential term is small. Altogether, the initial growth rate during time of the order of $\eta/\Delta P$ is very slow. This is the cause for the "delay time" observed in the numerical solutions of Proussevitch et al. [11] and discussed by Sparks [22] and Sahagian et al. [23]. We can now summarize this issue and state that viscous resistance of the melt poses the main inhibition to growth, while R is of the same magnitude as R_{CR}, but the actual size of the nucleus and its deviation from R_{CR} are also important.

It is important to verify our assumption that P_g remains close to its initial value, P_0. The difference between the two, $\delta P_g = P_0 - P_g$, is [20]:

$$\frac{d(\delta P_g)}{dt} = -\frac{3D\rho_m C_0}{2\rho_g}\cdot\frac{\delta P_g}{R_0^2\exp(\Delta P t/2\eta)} + \frac{3P_0\Delta P}{4\eta}. \tag{5}$$

The first term on the right-hand side of Eq. 5 describes the built-up of pressure due to diffusive mass flux. In the very initial stages, the concentration on the bubble wall is close to that of the supersaturated melt, $\delta P_g \sim 0$, diffusive flux is negligible, and pressure falls linearly due to expansion. Later on, and while time is still smaller than $\eta/\Delta P$, the first term grows until it almost cancels the second. The condition of zero gas pressure variation, or equivalence between the first and the second terms, while assuming $\exp(\Delta P t/2\eta) \approx 1$ yields:

$$\delta P_g = \frac{1}{2}\frac{\Delta P R_0^2}{\eta D}\frac{\rho_g P_0}{\rho_m C_0} = \frac{1}{2}Pe\frac{P_0^{3/2}M}{GT\rho_m K_H}. \tag{6}$$

With both Pe and $\rho_g/\rho_m C_0$ smaller than 1, the internal pressure in the bubble remains very close to P_0, as long as radial growth is small. The duration of this stage will be discussed below.

As growth accelerates, diffusive mass transfer cannot provide the flux needed to preserve the gas pressure. The above approximations break and internal pressure falls to just slightly above ambient pres-

sure. Even at this stage, where growth is controlled by the diffusive flux into the bubble, the diffusive time scale is shorter than the viscous time scale and the steady-state approximation, Eq. 2, is valid for moderate pressure drops. Under these conditions, Lyakhovsky et al. [17] developed an analytical solution for the growth of solitary bubbles:

$$R^2 = \frac{2D\rho_m(C_0 - C_f)}{\rho_g}t - \frac{2}{3}\frac{D\eta}{P_f}\frac{\rho_m}{\rho_g}(2C_0 + C_f)\log\left(\frac{\Delta P}{\eta}t\right). \quad (7)$$

At long times, the first term on the right-hand side is the dominant one and growth follows a square-root relation with an effective diffusion coefficient D_{eff}:

$$D_{eff} = \frac{2D\rho_m(C_0 - C_f)}{\rho_g}. \quad (8)$$

As can be seen in Fig. 1, R is bounded by two analytical curves: an exponent, Eq. 4, which describes the viscosity-controlled growth; and a square-root, Eqs. 7 and 8, which describes the diffusion-controlled stage. The transition from exponential to square-root growth is marked by the crossing of the two curves. At the time of crossing (τ_{vd}):

$$R_{CR} + (R_0 - R_{CR})\exp\left(\frac{\Delta P}{4\eta}\tau_{vd}\right) = \sqrt{D_{eff}\tau_{vd}}. \quad (9)$$

Assuming R_0 of a new nucleating bubble is 10% larger than R_{CR}, we obtain:

$$\frac{\Delta P\tau_{vd}}{\eta} = \frac{\tau_{vd}}{\tau_v} = 2\ln\frac{\Delta P\tau_{vd}}{\eta} - 2\ln\left(\frac{\sigma^2 M}{50GT\rho_m}\frac{P_f}{\Delta P}\frac{1}{\eta D(C_0 - C_f)}\right). \quad (10)$$

Eq. 10 cannot be solved explicitly, but as may be seen in Fig. 2, for a wide range of parameters τ_{vd} is of the order of $(10-60)\tau_v$ and may be approximated using the following relation:

$$\frac{\tau_{vd}}{\tau_v} \approx -15 + 10\ln(Pe). \quad (11)$$

Fig. 1 indicates that for growth under constant pressure the bubble closely follows the exponential curve for about $\tau_{vd}/2$. That means that water-rich rhyolite at depth of a few kilometers ($\eta < 10^6$ Pa s, $\Delta P \sim 10^8$ Pa, $\tau_v < 0.01$ s) will reach the square-root stage after less than a second. Bubbles in a highly viscous lava flow or dome ($\eta > 10^9$ Pa s, $\Delta P \sim 10^6$ Pa, $\tau_v > 1000$ s) may follow the exponential law and retain internal pressure for a few hours or even days.

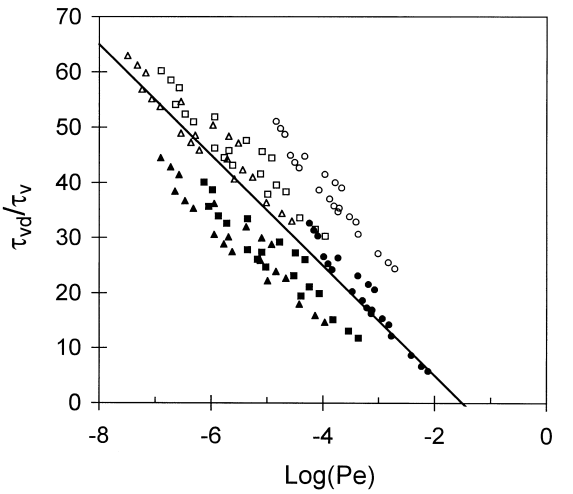

Fig. 2. The time-scale of transition from viscosity-controlled to diffusion-controlled growth normalized to the viscous time scale τ_v. Markers — exact solutions of (Eq. 9) for a range of conditions: P_0 varies from 150 to 0.2 MPa; $P_f = 0.9, 0.5, 0.1\ P_0$; R_{CR}, C_0, ρ_g and η calculated according to the Laplace equation, Henry's Law, the ideal gas law, and the relation of Schulze et al. [19], respectively; $D = 10^{-11}$ cm^2/s and $\rho_m = 2300$ kg/m^3. Open symbols — $R_0 = 1.01R_{CR}$, solid symbols — $R_0 = 2R_{CR}$, squares — $\sigma = 0.1$ N/m, $T = 1000$ K, triangles — $\sigma = 0.05$ N/m, $T = 1000$ K, circles — $\sigma = 0.1$ N/m, $T = 1200$ K. The line represents an approximate linear fit to the results (Eq. 11).

3. Experimental verification of the model

Lyakhovsky et al. [17] demonstrated the agreement between the model and experimental results at high pressure and temperatures. In their experiments viscosity was in the range of 10^4–10^5 Pa s and ΔP between 10 and 135 MPa. Under these conditions, τ_v is less than a second and experimental examination of the viscosity-controlled regime is impossible. Vesiculation experiments on water-poor natural rhyolites [1,24] allow testing the model during the first, viscosity-controlled stage and during the transition to the diffusion-controlled stage. We also present new experimental data where degassing takes place along extreme concentration gradients. Such experiments

allow testing the model under extreme conditions where the variation of viscosity along the concentration profile is important and where the "steady-state diffusion" approximation is not valid and the equation of diffusion has to be fully solved. All these experiments examine growth under constant pressure. At a first glance, this may disappointing, as in the natural case pressure decreases during eruptions. However, it must be noted that once the role of the various parameters is understood and determined, the extension of the model to the case of variable pressure is straight forward.

3.1. Bubble growth in water-poor rhyolite

Murase and McBirney [24] were the first to follow the growth of bubbles in slabs of Newberry Rhyolitic Obsidian heated to 1050ºC at 1 bar. Their plot of radius versus time follows the sigmoidal shape. It rises exponentially for the first 30 min, then growth decelerates for ~50 min, and finally, the bubbles shrink, most probably due to diffusion through the surface of the thin slabs. Using the viscosity measured by Murase and McBirney ([24], 10^7 Pa s at 1050ºC) and estimating vapour pressure of the order of a few bars (corresponding to the initial water content of the rhyolite), we calculate τ_v of the order of 30–100 s, and τ_{vd} (Eq. 11) of the order of 1000–4000 s. The bubbles are expected to follow the exponential curve for about $\tau_{vd}/2$, as they really do during the initial stages of the experiments.

Bagdassarov et al. [1] followed the experimental method of Murase and McBirney [24], but used a video camera to monitor continuously the growth of individual, pre-existing bubbles in a rhyolitic obsidian at 650–925ºC. They also monitored the vesiculating melt dilatometrically. The obsidian they used contained 0.14% water, corresponding to saturation pressure of 2 bars. When heated at room pressure, ΔP is 1 bar (10^5 Pa). The measured viscosity of the obsidian at this temperature range (as measured independently by them) was 5×10^5 to 5×10^9 Pa s, resulting τ_v of 5–50 000 s and τ_{vd}, about an order of magnitude longer. Plotting the log of the bubble radius, R (normalized to initial radius, R_0, which varied between 10 and 50 μm), we obtain a series of straight lines for the region $t < \tau_{vd}$ (Fig. 3). Comparing these results with (Eq. 4 and remembering

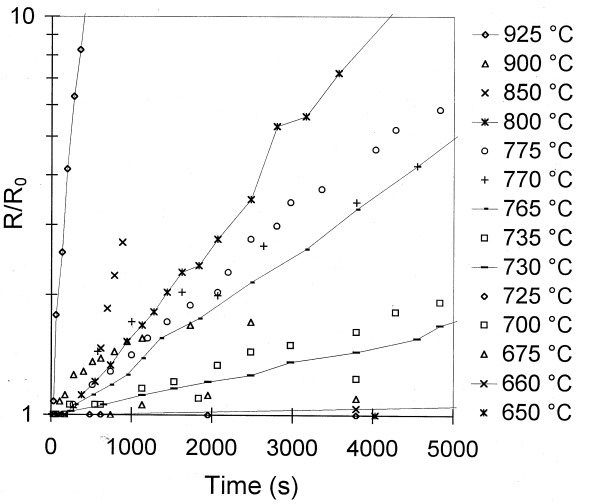

Fig. 3. Bubble growth in the high-viscosity, low-supersaturation regime. The experimental data of Bagdassarov et al. [1] was replotted on a semi-logarithmic plot, where the straight lines correspond to exponential growth in agreement with (Eq. 4).

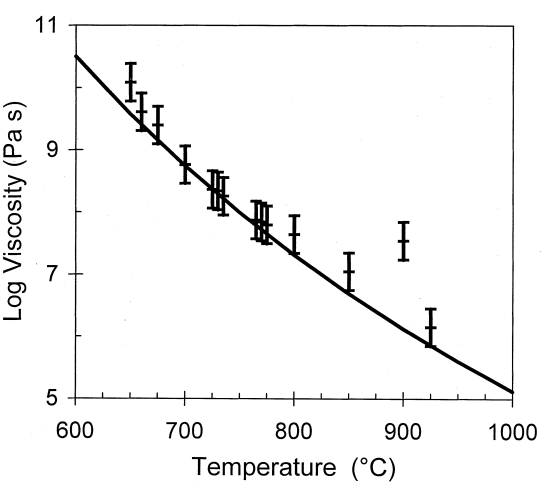

Fig. 4. Viscosities calculated based on growth systematics using the slopes of the lines in Fig. 3 compared with those given by the best fit to the micropenetration data (table 3 of Bagdassarov et al. [1]).

that in their experiments $R_0 \gg R_c$, the slope of the straight lines should correspond to $\Delta P/4\eta$. Knowing ΔP, we used the slopes of the lines to derive melt viscosity. Fig. 4 illustrates the excellent agreement between viscosity calculated using our model and that determined from micro-penetration experiments on the same sample [1].

Bagdassarov et al. [1] also characterized a "lag time" which they defined as the time between attainment of run temperature and the time at which the radius of the bubble increased by 5%. They noted that it varies with temperature according to:

$$\log(\tau_{\rm lag}) = -12.36 + 14\,950/T.$$

The activation energy for the lag time is identical to that for viscous flow [1]:

$$\log \eta = -6.629 + 14\,957/T.$$

They related the similarity to shape relaxation of the initial bubbles, but as shown here, it can be fully explained by the growth model, as the time it takes to grow from R_0 to 1.05 R_0. Using Eq. 4 with $R_0 \gg R_{\rm CR}$, $R/R_0 = 1.05$, $\Delta P = 10^5$ Pa [1] and the above expression for viscosity, the lag time is:

$$\log_{10}(\tau_{\rm lag}) = \log_{10}(4\ln(1.05)/\Delta P) + \log_{10}\eta$$
$$= -12.33 + 14\,957/T,$$

surprisingly close to the fit of the experimentally measured lag time data.

As a matter of fact, growth systematics may be used in order to determine the viscosity of high viscosity melts and glasses. If the solubility of water (or other volatiles) and the corresponding saturation pressure are known, growth should follow Eq. 4 for about $10\eta/\Delta P$, and for pressures in the range of 1 MPa, viscosities of the order of 10^7–10^{11} Pa s may be determined accurately.

3.2. Bubble growth in water-rich rhyolite: high peclet numbers and variable viscosity

The design of the experiments we performed is similar to that of the heating stage experiments of Bagdassarov et al. [1], but glasses were pre-hydrated to 5 wt% water. Stevenson et al. [25] also examined vesiculation of hydrated rhyolites (1.8 wt%). However, their volumetric measurements provide no data on the radius of the bubbles or the separation between them. Slabs of rhyolitic obsidian from Little Glass Butte, Oregon (LGB) were used as a starting material. They were placed in open gold capsules and covered with gold caps together with powdered glass of the same composition in order to prevent dissolution of the slabs. Capsules were loaded in rapid-quench, cold-seal, pressure vessels (see [26], for further details and for composition of rhyolite) and held at 140 MPa, 850ºC for four days. Then, bubbles were nucleated by dropping the pressure to 70 MPa for ~3 s, after which the sample was quenched rapidly under pressure. The resulted sample was clear, colourless, and carried very few zircon crystals and just a few bubbles, 3–10 μm in size. It was cut to small pieces (~2 mm in size) and doubly polished to a thickness of ~0.8 mm. Water content of the glass was determined spectroscopically as 5.0 ± 0.1 wt% (using a Nicolet 740 FTIR and the calibration of Newman et al. [27]).

The small, transparent samples were placed on a quartz stage inside the platinum heater of a heating stage [28]. Temperature was set using a variable transformer and monitored using a chromel-alumel thermocouple located just under the quartz stage. Former calibrations gave accurate readings (±5ºC) for the melting temperatures of Pb, KI, NaCl and Au. The sample was monitored using a 20×, superlong working distance lens. The whole experiment was monitored by a video-recorder connected to two cameras, one mounted on the microscope and recording the experiment (resolution of 0.8 μm/line) and the other recording the thermometer readings and the time.

The experimental conditions and parameters used in the numerical calculations are listed in Table 1.

Table 1
Experimental conditions

Run #	C_0 (wt%)	T [a] (ºC)	R_0 [b] (μm)	η_0 [c] (Pa s)	D [d] (m^2/s)	Pe Eq. 1
AC25a	5.0	460	10.0	6.8×10^7	5×10^{-12}	40
AC25b [e]	4.2	460	1.0	1.7×10^8	5×10^{-12}	0.1
AC26	5.0	400	8.0	6.9×10^8	6×10^{-13}	20
AC27	5.0	375	4.5	1.6×10^9	6×10^{-13}	3

[a] Temperature is constant to ±5ºC (see Fig. 5a).
[b] Initial bubble radii for simulation.
[c] Viscosity for initial water content calculated as 0.1 of that given by [19].
[d] Diffusion coefficient (adjusted parameter).
[e] The data refer to a bubble that was non-visible in the beginning of the experiment. The record starts when the bubble was first observed ($R_0 = 1$ μm), 50 μm away from the bubble described at AC25a. Water content and initial viscosity were calculated using the model run for AC25a.

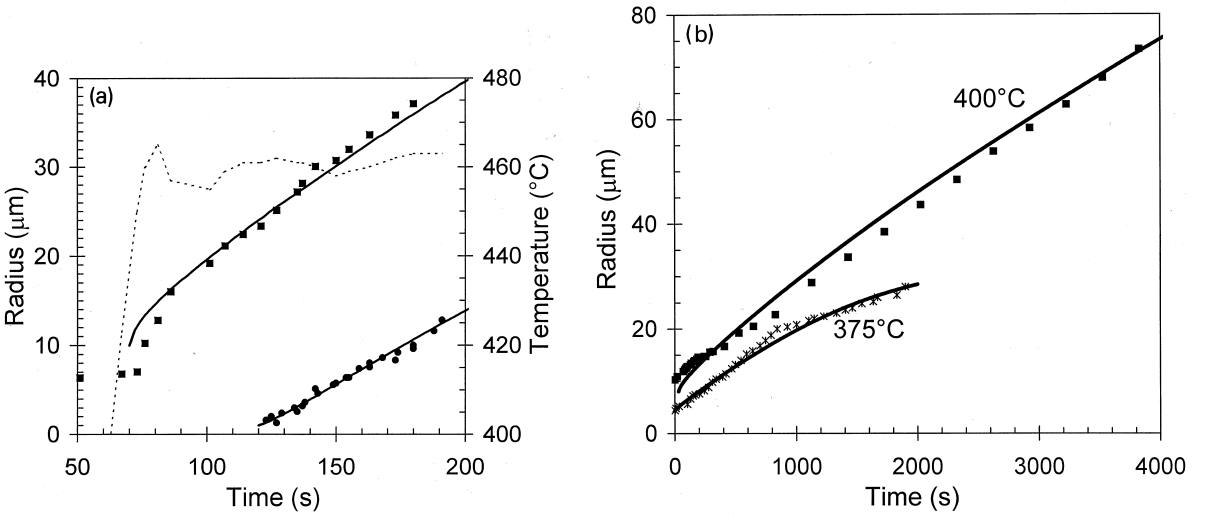

Fig. 5. Heating-stage experiments at the high-viscosity, high-supersaturation regime. (a) Growth of two bubbles in a single run (AC25). The smaller bubble appeared about 50 s after the first began growing (~120 s after beginning of heating). The distance between the bubbles was 50 μm. Solid lines — numerical simulation of the growth using the parameters given in Table 1. Dashed line — temperature during the experiment. (b) The growth of single bubbles in two separated experiments at 375 and 400ºC.

The results are presented in Fig. 5. Plotting $\ln(R/R_0)$ vs. time did not yield straight lines. This is the result of the high supersaturation and relatively large initial bubble radii that led to $Pe > 1$. The approximations that led to Eq. 4 are no longer valid and a full solution of the diffusion equation was employed in the numerical simulation. We also accounted for the difference in temperature between the hydration at high pressure (850ºC) and the heating-stage experiment (375–460ºC).

We modified the numerical code used by Lyakhovsky et al. [17] so that viscosity and diffusivity may be varied as functions of water concentration with radial distance from the growing bubble. Due to the contrasting models of the dependence of water diffusion on water concentration in the melt [29,30], we chose, at this stage, to keep this parameter constant. The viscosity of silicate melts increases substantially during dehydration [18,19]. At low temperatures and high water contents these two parameterizations of viscosity differ by 1–2 orders of magnitude. The observed rates of bubble growth (Fig. 5) suggest that the equation of Hess and Dingwell [18] significantly overestimates the effective melt viscosity. At 375ºC and 5 wt% water (run AC27, Table 1) they predict $\eta = 2 \times 10^{12}$ Pa s. Even if melt viscosity is assumed to be constant, with no increase due to dehydration, Eq. 4 predicts growth from initial radius of 3.5 μm to only 3.57 μm during the first 500 s. The observed bubble (Fig. 5a) grew to 15 μm during that time. Similar estimation for the bubble in AC25a (460ºC, 5 wt% water) predicts growth from 6 to 8.4 μm in 50 s, while the bubble actually grew to more than 20 μm. Viscosities predicted by Schulze et al. [19] are lower by 1–2 orders of magnitude. Still, they underestimate the initial growth rates. We found that good fits are obtained using viscosities that are a factor ten lower than those calculated using the equation of Schulze et al. [19] for given temperatures and water contents (Fig. 5). These lower viscosities may reflect the higher alkali content of the rhyolite we used and its lower degree of polymerization.

The modified code solves for the water content along the radial profile, calculates the corresponding viscosities, and solves the Navier–Stokes equation accounting for this spatial variation. Examination of the numerical simulations reveals that the more viscous, dehydrated layer around the bubble puts the main constrain on growth. Using the initial parameters given in Table 1, good fits are obtained for the growth of pre-existing bubbles at three different temperatures (Fig. 5). In run HS-25, an additional small bubble appeared in the field of view about

50 s after the first bubble started growing. Using the observed distance between the bubbles (~50 μm) and the calculated profile of water concentration, we estimated the concentration of water as 4.2 wt% at the location where the additional bubble appeared, at the time it was first observed. Using this water content and the observed separation it was possible to fit the simultaneous growth of the two bubbles using identical parameters.

4. Discussion

The slow growth rate at the initial stages of bubble evolution was noticed by early modellers of bubble growth (e.g. [31] and references therein). Many of these early works modeled low viscosity liquids and attributed the slow initial growth rate to the effect of surface tension. Sparks [31] suggested that in geological systems, both surface tension and viscosity may be important in controlling the initial growth rate. He estimated time delays of the order of tens of seconds in viscous obsidian.

Slow initial growth rates were obtained in the numerical solutions of Toramaru [9] and Proussevitch et al. [11]. The latter authors attributed the phenomenon to the effect of surface tension, but as shown later [22,23], it is mainly the result of high melt viscosity. Recently, Toramaru [10] obtained an exponential growth law for the initial stages of growth in highly viscous melts, which converges with our approximate solution (Eq. 4) if R_{CR} is negligible relative to R_0. As demonstrated by (Eq. 4), surface tension does play a limited role and since most bubbles nucleate with $R_0 \sim R_{CR}$, the pre-exponential term, which is the difference between the two, may be much smaller than R_0 itself, leading to a much slower initial growth rate.

Recent experimental data [1,17] and the experiments presented here, combined with the model outlined here and in Lyakhovsky et al. [17] constitute the first experimentally verified model of bubble growth. The good agreement between numerical simulations and approximate analytical solutions assures that the physics of growth and the role of the various controlling parameters are well understood. The current model can account for variation in viscosity and water diffusivity during dehydration and may be used to model growth under either constant or variable pressure.

5. Geological applications

Slow initial growth rates are only important if melt viscosity is high enough, of the order of 10^7 Pa s or higher. Such high viscosities are reached only in degassed melts, with water content of less than 1 wt% [18,19]. These low concentrations may be achieved at shallow depths, e.g., during the final stages of flow in the conduit, in hot pumice, and in lava flows and domes of silicic composition.

6. Bubble growth before and after fragmentation

Along most of their ascent in the conduit, melts can degas efficiently [10,20], so that their water content is determined by the ambient pressure. As shown by [20], the disequilibrium encountered by Proussevitch and Sahagian [15] is the result of the extremely low number density of bubbles used in their simulation. Further up the conduit, shortly before fragmentation, the melt accelerates [12,32]. At this stage, the viscosity of the degassed melt is relatively high. The combination of high viscosity and fast drop of pressure prevents equilibrium degassing ([10] and Lyakhovsky and Navon, unpublished data). Away from existing bubbles, melt may become supersaturated, so that in principle, new bubbles may nucleate. As shown here, even if such nucleation does take place, it will have a limited effect on fragmentation, since these newly nucleating bubbles would have almost no time to grow. If indeed, velocities just below fragmentation are high [12], the newly nucleated bubbles have less than a minute to grow. Numerical simulations suggest that for bubble number density of 10^{12} m^{-3} and ascent rate of 1 m/s supersaturation develops only when water content is ~1% and viscosity is in the range of 10^7–10^8 Pa s [20]. The maximum supersaturation is less than 5 MPa so that it takes more than a minute for a bubble to grow from 1.1 R_{CR} to 10 μm if $\eta = 10^7$ Pa s. It takes more than 10 min if $\eta = 10^8$ Pa s, so no such bubbles are expected. Actual number densities of bubbles in pumice are commonly higher than 10^6

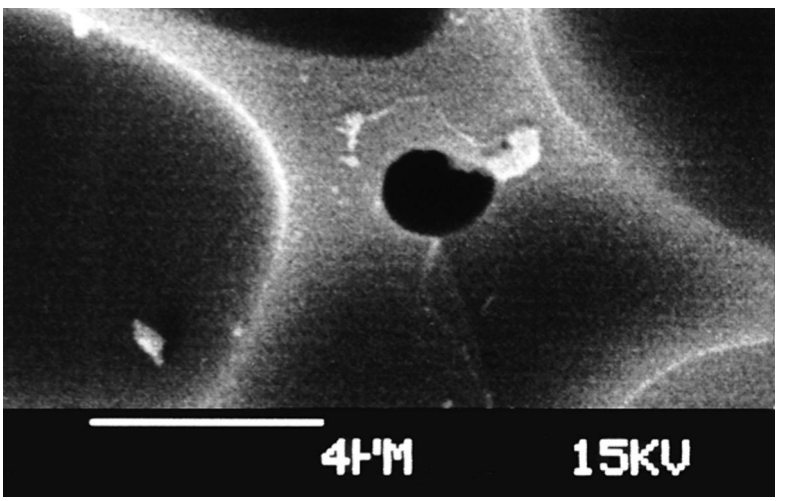

Fig. 6. A tiny bubble (~2 μm in diameter) in a melt pocket between much larger bubbles (10–30 μm) in a fragment of pumice from Lipari (Photo by M. Hilton).

cm^{-3}, so that it may be expected that supersaturation is reached only at shallower levels where pressure is lower, viscosity is higher, and growth is even slower.

In pumice, tiny spherical bubbles are sometimes observed in the relatively thick melt pockets between larger bubbles. Fig. 6 presents a typical bubble from rhyolitic pumice from Lipari. Other examples are small bubbles (<5 μm) in fig. 1a of Klug and Cashman [33], the small bubble below the centre of fig. 19 of Cashman and Mangan [34], and perhaps, the small bubbles indicated by the data of Sparks and Brazier [35]. It is possible that these bubbles are the result of late nucleation shortly before, or immediately after fragmentation. The evolution of such bubbles depends on the time–temperature–viscosity path followed by the fragment (e.g. [13]) and their presence may be used to constrain the viscosity at fragmentation or the time between fragmentation and quenching of the pumice.

Using the estimation of Thomas et al. [13] for pressure and viscosity at fragmentation, we calculate the time needed to develop bubbles of 0.1–10 μm in size in pumice fragments (Table 2). If indeed, the quenching time is less than 1 s, as suggested by Thomas et al. [13], no bubbles could have grown in the pumice of any of these eruptions after fragmentation. If they are found in the Minoan and the Taupo/Hatepe, but not in the Bishop, they may indicate that growth time was longer, or viscosities lower than those assumed. The presence of such bubbles in Mount St. Helens and Lipari pumice suggests that viscosities were lower than 10^7 Pa s (and corresponding water content of more than 1 wt%) at fragmentation, or that bubbles nucleated more than 10 s before fragmentation. Further study of such bubbles may provide a probe for the conditions at fragmentation.

7. Lava domes

Lava domes are formed by effusion of partially degassed, viscous, dacitic to rhyolitic magma. The mechanism by which the magma lost most of its water is still debated [36,37], but the extruding magma still contains 0.2–1 wt% water and forms domes with typical thickness of tens of meters [38,39]. The exposure of such magmas to atmospheric pressure should lead to expansion of existing bubbles and may cause nucleation and growth of bubbles in highly viscous, cooling lava.

We use the model to examine two interesting observations. The first is the instantaneous explosive fragmentation of blocks falling from the lava dome of Mount Unzen, which resulted in Merapi-type pyroclastic flows in 1991 [6]. Sato et al. [6] suggested that “variable degrees of degassing of the magma produces a wide range of pore pressures in the ex-

Table 2
Growth time from nucleation at fragmentation

Magma	η [a] (Pa s)	Water [a] (wt%)	P_{frag} [b] (MPa)	R (μm)	0.1	1	10	1	1
				R_0/R_{CR}	1.1	1.1	1.1	1.01	2
				R_{CR} [c] (μm)	Time to grow from R_0 to R [d] (s)				
Minoan	9×10^6	1.5	12.0	0.017	12	19	26	26	12
Hatepe	1×10^7	1.6	13.7	0.015	12	19	26	26	12
Taupo	2×10^7	1.6	13.7	0.015	24	38	52	52	25
Bishop	2×10^8	1.8	17.3	0.012	201	312	420	419	206

[a] Viscosities and water content at fragmentation from [13]. A more recent compilation [43] estimates similar numbers.
[b] P_{frag} is calculated using the water content of the previous column and Henry constant of 4.33×10^{-6} [26].
[c] R_{CR} calculated as $2\sigma/\Delta P$ with $\sigma = 0.1$ N/m [41].
[d] Times were calculated assuming exponential growth (Eq. 4) for various choices or R_0 and R, as given in the upper two rows.

truded lava domes". Fink and Kieffer [7] estimated that pressures of 1–10 MPa are sufficient to accelerate fragments to velocities up to 100 m/s. Barclay et al. [14] criticized this model, pointing out that such internal pressures may only be reached if the water content of the melt is high enough (1.3 wt% for 10 MPa, 0.4% for 1 MPa). Using their expanding shell model, they calculated that the viscosity of such melts is insufficient for keeping the pressure for more than a few hours (fig. 3 of [14]). The present model allows a more detailed examination of internal pressures in the bubbles following dome extrusion.

The second observation is that of Cashman and Taggart [40], who described the evolution of flow morphology of the dacite dome of Mount St. Helens and noted: "Lava less than 24 hours old has a smooth, coherent surface. As the lava moves downslope and its rate of movement decreases, its surface becomes rough and fragmented". Anderson and Fink [38] found that the transformation from smooth to scoriaceous surface depends on the slope and the water content of the extruded lava. They suggested that "Volatile contents of around 0.3 to 0.4 wt% allow vesiculation of lava at the surface or slightly beneath the initially smooth crease structure walls, forming surface scoria". The 1 day time scale of surface evolution documented at Mount St. Helens may be explained by our model.

Consider a very simple dome model, where lava with low initial water extrudes and forms a flat dome, which cools from above (half space with initial temperature of 750°C and constant surface temperature of 27°C). Knowing the temperature and pressure as a function of depth and time, we can estimate supersaturation, viscosity, diffusivity and then τ_{vd}, which provides a good estimate of the time during which the pressure in the bubbles is in excess of the ambient pressure at a certain depth, z.

We chose initial water content of 0.4 wt% water, similar to that estimated for the Mt. St. Helens dome [38]. This corresponds to saturation under pressure of 0.96 MPa, or last equilibration at ~40 m depth. When emplaced at 1 m depth, ΔP is 0.94 MPa ($0.96 - \rho g z$). Viscosities were calculated using the equation of Schulze et al. [19]. Using the expression of Hess and Dingwell [18], or accounting for the effect of crystals on magma viscosity would yield higher values. The relatively low initial temperature we chose (750°C) partially compensates for that, but we note that higher viscosities would enhance the ability of the dome to store pressurized bubbles. The initial viscosity is 4.3×10^9 Pa s [19] and τ_v is at least 5000 s. Using initial diffusivity of 2.5×10^{-12} m^2/s [29] and surface tension of 0.1 N/m [41], we calculated an initial τ_{vd} (at nucleation) of 3.7×10^5 s, or about 4 days. However, during these four days the melt cools and its viscosity increases. This leads to a longer τ_{vd} and the bubbles keep their pressure for even longer time.

Fig. 7 displays τ_{vd} as a function of time for various depths in the dome. At the upper left part of the figure, $t < \tau_{vd}$, bubble growth is exponential, and the bubbles maintain high internal pressures. At the lower right $t > \tau_{vd}$ and the pressure in the bubbles is relaxed to the ambient pressure at depth. The transition between the two regimes is fast (of the order of τ_{vd}, Fig. 1) so that the $t = \tau_{vd}$ line provides a good estimation for the time when the

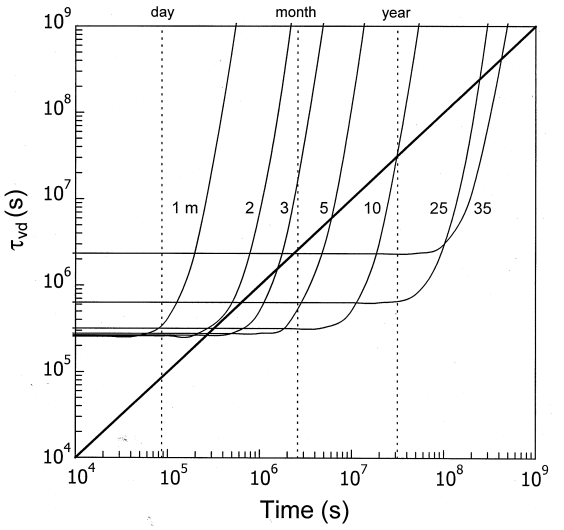

Fig. 7. The approximate time during which the internal pressure is preserved in newly nucleated bubbles, τ_{vd}, Eq. 9, in a cooling lava dome with initial water content of 0.4 wt%. Numbers next to curve denote the depth beneath the surface of the dome. At 1 m depth τ_{vd} is initially 2.5×10^5 s, but as cooling starts after 7×10^4 s, viscosity quickly increase and τ_{vd} grows longer and is never reached (time is always shorter than τ_{vd}). In this case, bubbles remain under pressure until gas temperature falls substantially. At 10 m depth, initial τ_{vd} is somewhat longer (3×10^5 s), due to the higher lithostatic pressure and smaller ΔP. However, cooling begins only after 10^7 s, so that τ_{vd} is exceeded and bubbles lose their internal pressure. The diagonal solid line separates the regime where τ_{vd} is never reached and pressure is preserved (on the upper left) from that where time exceeds τ_{vd} and pressure is lost (lower right).

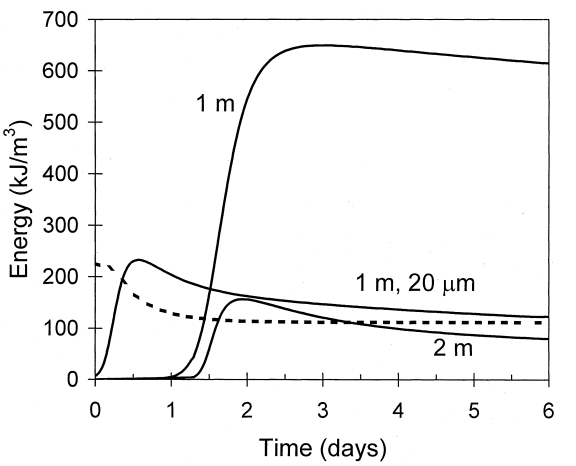

Fig. 8. The energy stored in 1 m^3 of a vesiculating dome. Solid curves — energy due to internal pressure in bubbles. If bubbles are nucleating at 1 or 2 m depth, the energy is small during the first day due to the very small size of the bubbles, it peaks after 2–3 days and decays slowly due to cooling of the gas. Pressure in 20 μm sized, pre-existing bubbles at 1 m depth falls faster and their stored energy peaks at a lower value during the first day. Dashed line — gravitational energy for a 10 m fall. The gravitational energy (per unit volume) falls with increasing vesicularity. All curves were calculated for 50% final vesicularity.

internal pressure in the bubbles falls. At 1 m depth, cooling is fast, viscosity increases and τ_{vd} quickly grows longer, so that t is always shorter than τ_{vd} and the bubbles maintain their pressure. Deeper down, cooling is slower, the $t = \tau_{vd}$ line is crossed and the pressure in the bubbles relaxes to the lithostatic pressure. The increase in the initial τ_{vd} with depth reflects the decrease in ΔP. In this simplified model, equilibrium solubility is reached at a depth of 39 m and no vesiculation takes place.

Examination of the situation for melt with 0.2 wt% water indicates that for all depths, $t < \tau_{vd}$, all curves fall in the upper left half of the plot (not shown), and bubbles do not grow to an appreciable size. Assuming similar viscosity for the Mt. St. Helens dome, this result may explain why the more degassed domes, with 0.2% water tend to keep their smooth surface. If water content is higher, subsurface expansion due to growth of bubbles may lead to disruption of the smooth surface after about a day.

Using the numerical model, we can simulate the evolution of bubble size and internal pressure during the cooling of the dome. Using these data, we can calculate the energy stored in the bubbles, so that in addition to a more accurate calculation of the time at which the stored energy reaches a maximum, we can also compare the energy stored in the compressed bubbles with gravitational and thermal energy. Fig. 8 presents the maximum work that may be done by the bubbles during isothermal, reversible expansion to atmospheric pressure:

$$E_{ex} = nGT \ln\left(\frac{P_g}{P_{atm}}\right).$$

Adiabatic expansion yields only about 20% less energy at the pressures of interest.

If E_{ex} is calculated for 1 m^3, then the number of moles is $n = 4\pi R^3 N_d P_g / 3GT$, where N_d is the number density of bubbles in the lava. In order to

compare the energy stored in new or pre-existing bubbles at depths of 1 and 2 m, we chose to adjust the number density, so that the final vesicularity is 50% in all cases (N_d is 10^6 and 10^7 for newly nucleated bubbles at 1 and 2 m, respectively). The initial τ_{vd} is similar at both depth, but cooling by 50° takes about 2 days at 1 m, and 7 days at 2 m (Fig. 8). Pressure fall begins after 1.5 days but is halted at ~0.65 MPa due to the fast cooling at 1 m. At 2 m, temperature remains high and pressure loss is almost complete after 4 days. As a result, the stored energy is much higher at 1 m. It remains high for more than a week and eventually decreases as pressure falls with falling temperature. Closer to the surface (e.g. at 0.5 m) cooling is even faster, bubbles do not have enough time to grow and the stored energy is lower. Increase in the initial melt viscosity or faster increase of viscosity (for example due to crystallization) will shift the depth of maximum stored energy to deeper depth. Crystallization may also lead to higher supersaturation and maintain high pressure in the bubbles for even longer times.

If the intruding melt carries bubbles, the evolution is faster. Also shown in Fig. 8 is the evolution of stored energy in pre-existing bubbles with initial radius of 20 μm, after exposure to lithostatic pressure at 1 m. Pressure quickly falls and stored energy peaks after half a day. It then starts falling until after ~2 days the increasing viscosity keeps it at a relatively constant value.

The energy stored at the pressurized magma is not trivial. The gravitational energy released during a fall of 10 m is up to 230 kJ/m^3 (depending on vesicularity), of the same order as that stored in the bubbles. The thermal energy is much higher, of the order of 10^6 kJ/m^3, but cannot be released before the lava is fragmented. Thus we conclude that the high internal pressure in the bubbles is an important source of energy for initiating pyroclastic flows following dome collapse. Energy that is of the order of magnitude of gravitational energy may be stored for days or even weeks and may lead to explosive disintegration of the dome rocks. The disintegration of lava blocks in the Unzen dome [6] may be the result of such a mechanism. The trigger for disintegration may be a gravitational instability or initiation of cracks as the magma cools, dehydrates and crystallizes. The role of the pressurized bubbles is to ensure efficient disintegration of the collapsing blocks (cf. [42]) and allow efficient release of thermal energy and initiation of a pyroclastic flow.

8. Conclusions

Bubble growth in highly viscous melts (>10^8 Pa s) is controlled by melt viscosity and the supersaturation pressure. During the initial stages of growth under constant pressure, pressure is maintained close to its initial value, and growth is approximately exponential. Later, pressure falls, radial growth is limited by diffusion and approaches the square root of time. The time of transition between the two regimes, τ_{vd}, depends on the decompression, melt viscosity, and the Peclet number of the system.

Numerical simulations produce close fit of the experimental data of Bagdassarov et al. [1] and validate the model for the high viscosity, low supersaturation regime. The role of variable viscosity along the concentration profiles around the bubbles was also examined by comparing the model with experiments at high viscosity and high supersaturation. The excellent agreement with analytical solution of end-member cases ensures that the physics of the process and the role of the various parameters are well understood.

Near-surface, degassed, silicic melts are viscous enough, so that viscosity controlled growth may last for minutes and even hours or days. Using the approximations developed here, we have shown that bubbles that nucleate shortly before fragmentation cannot grow fast enough to be important during fragmentation. We suggest that tiny bubbles observed in melt pockets between large bubbles in pumice represent a second nucleation event shortly before or after fragmentation. The presence of such bubbles indicates the conditions at fragmentation.

The model may also be used to follow the growth of bubbles in viscous lava domes. The water content of the extruded melt is a key factor in their evolution. Melts of low water content (<0.2 wt%) are too viscous and bubbles nucleated in them will not grow to an appreciable size. Bubbles may grow in melts with ~0.4 wt% water and preserve their internal pressure for days. The energy stored in such bubbles may be important during dome collapse and

pyroclastic flow formation. Melts with higher water content should grow bubbles fast enough so that the internal pressure in them relaxes rapidly to the lithostatic value.

Acknowledgements

Some of the ideas presented in this paper were shaped during Navon's summer visit to the University of Bristol supported by the Leverhulme Foundation. Discussions with Matt Hilton, Jenny Barclay, Anne-Marie Lejeune, and Jon Fink and reviews by Steve Sparks, Don Dingwell and an anonymous reviewer are gratefully acknowledged. The Project is supported by the Isreal—US Binational Science Foundation. Support from the Ministry of Absorption (A.C. and V.L. Giladi Program) and the Ministry of Science (A.C.) are gratefully acknowledged. ***[FA]***

Appendix A. Notation list

C	concentration of water in melt (wt%)
D	diffusion coefficient of water in melt (m^2/s)
E	energy (J)
G	the gas constant (J/mol K)
K_H	Henry's constant (Pa)
M	molecular weight of water (kg/mol)
n	number of moles of water
N_d	bubble number density (m^{-3})
P	pressure (Pa)
Pe	Peclet number
r	radial coordinate (m)
R	bubble radius (m)
t	times
T	temperature (ºC)
ΔP	supersaturation pressure (Pa)
η	melt viscosity (Pa s)
ρ	density (kg/m^3)
σ	surface tension (N/m)
τ	characteristic time (s)

Subscripts

0	initial value
CR	critical
d	diffusive
f	final value
g	gas
m	melt (liquid silicate)
R	properties of the bubble melt interface
v	viscous
vd	viscous-diffusive transition

References

[1] N.S. Bagdassarov, D.B. Dingwell, M.C. Wilding, Rhyolite magma degassing: an experimental study of melt vesiculation, Bull. Volcanol. 57 (1996) 587–601.
[2] D.A. Swanson, D. Dzurisin, R.T. Holcomb, E.Y. Iwatsubo, W.W. Chadwick, T.J. Casadevall, J.W. Ewert, C.C. Heliker, Growth of the lava dome at Mount St. Helens, Washington (USA), 1981–1983, in: J.H. Fink (Ed.), The Emplacement of Silicic Domes and Lava Flows, Geol. Soc. Am. Spec. Pap. 212 (1987) 1–16.
[3] J. Fink, Volcano warning needed, Nature 351 (1991) 611.
[4] S. Nakada, T. Fujii, Preliminary report on the activity at Unzen Volcano (Japan), November 1990–November 1991: Dacite lava domes and pyroclastic flows, J. Volcanol. Geotherm. Res. 54 (1993) 319–333.
[5] S. Young, S. Sparks, R. Robertson, L. Lynch, W. Aspinall, Eruption of Soufriere Hills Volcano in Montserrat continues, Eos, Trans. Am. Geophys. Union 78 (1997) 401–409.
[6] H. Sato, T. Fujii, S. Nakada, Crumbling of dacite dome lava and generation of pyroclastic flows at Unzen volcano, Nature 360 (1992) 664–666.
[7] J.H. Fink, S.W. Kieffer, Estimate of pyroclastic flow velocities resulting from explosive decompression of lava domes, Nature 363 (1993) 612–615.
[8] J.C. Eichelberger, Silicic volcanism: ascent of viscous magmas from crustal reservoirs, Annu. Rev. Earth Planet. Sci. 23 (1995) 41–63.
[9] A. Toramaru, Vesiculation process and bubble size distribution in ascending magmas with constant velocities, J. Geophys. Res. 94 (1989) 17523–17542.
[10] A. Toramaru, Numerical study of nucleation and growth of bubbles in viscous magmas, J. Geophys. Res. 100 (1995) 1913–1931.
[11] A.A. Proussevitch, D.L. Sahagian, A.T. Anderson, Dynamics of diffusive bubble growth in magmas: Isothermal case, J. Geophys. Res. 98 (1993) 22283–22307.
[12] R.S.J. Sparks, J. Barclay, C. Jaupart, H.M. Mader, J.C. Phillips, Physical aspects of magmatic degassing I. Experimental and theoretical constraints on vesiculation, Rev. Mineral. 30 (1994) 413–445.
[13] N. Thomas, C. Jaupart, S. Vergniolle, On the vesicularity of pumice, J. Geophys. Res. 99 (1994) 15633–15644.
[14] J. Barclay, D.S. Riley, R.S.J. Sparks, Analytical models for bubble growth during decompression of high viscosity magmas, Bull. Volcanol. 57 (1995) 422–431.
[15] A.A. Proussevitch, D.L. Sahagian, Dynamics of coupled diffusive and compressive bubble growth in magmatic systems, J. Geophys. Res. 101 (1996) 17447–17455.
[16] E. Kaminski, C. Jaupart, Expansion and quenching of vesicular magma fragments in Plinian eruptions, J. Geophys. Res. 102 (1997) 12187–12203.
[17] V. Lyakhovsky, S. Hurwitz, O. Navon, Bubble growth in rhyolitic melts: experimental and numerical investigation, Bull. Volcanol. 58 (1996) 19–32.
[18] K-U. Hess, D.B. Dingwell, Viscosities of hydrous

leucogranitic melts: a non-Arrenian model, Am. Mineral. 81 (1996) 1297–1300.
[19] F. Schulze, H. Behrens, F. Holz, J. Roux, W. Johannes, The influence of water on the viscosity of a haplogranitic melt, Am. Mineral. 81 (1996) 1155–1165.
[20] O. Navon, V. Lyakhovsky, Vesiculation processes in silicic magmas, in: J.S. Gilbert, R.S.J. Sparks (Eds.), Physics of Explosive Volcanism, Geol. Soc. London Spec. Publ. (in press).
[21] E. Stolper, Water in silicate glasses: an infrared spectroscopic study, Contrib. Mineral. Petrol. 81 (1982) 1–17.
[22] R.S.J. Sparks, Comment on "Dynamics of diffusive bubble growth in magmas: Isothermal case", J. Geophys. Res. 99 (1994) 17,827–17,828.
[23] D.L. Sahagian, A.A. Proussevitch, A.T. Anderson, Reply on Comment on "Dynamics of diffusive bubble growth in magmas: Isothermal case", J. Geophys. Res. 99 (1994) 17,829–17,832.
[24] T. Murase, A. McBirney, Properties of some common igneous rocks and their melts at high temperatures, Geol. Soc. Am. Bull. 84 (1973) 3536–3592.
[25] R.J. Stevenson, N.S. Bagdassarov, C. Romano, Vesiculation processes in a water-rich calc-alkaline obsidian, Earth Planet. Sci. Lett. 146 (1997) 555–571.
[26] S. Hurwitz, O. Navon, Bubble nucleation in rhyolitic melts: experiments at high pressure, temperature and water content, Earth Planet. Sci. Lett. 122 (1994) 267–280.
[27] S. Newman, S. Epstein, E.M. Stolper, Water, carbon dioxide and hydrogen isotopes in glasses from the ca. 1340 A.D. eruption of the Mono Craters, California: constraints on degassing phenomena and initial volatile content, J. Volcanol. Geotherm. Res. 35 (1988) 75–96.
[28] S.A. Zapunnyy, A.V. Sobolev, A.A. Bogdanov, A.B. Slutzky, L.V. Dmitriev, L.L. Kunin, An apparatus for high-temperature optical research with controlled oxygen fugacity, Geochem. Int. 26 (1989) 120–128.
[29] Y. Zhang, E.M. Stolper, G.J. Wasserburg, Diffusion of water in rhyolitic glasses, Geochim. Cosmochim. Acta 55 (1991) 441–456.
[30] M. Novak, H. Behrens, An experimental investigation on diffusion of water in haplogranitic melts, Contrib. Mineral. Petrol. 126 (1996) 365–376.
[31] R.S.J. Sparks, The dynamics of bubble formation and growth in magmas: a review and analysis, J. Volcanol. Geotherm. Res. 3 (1978) 1–37.
[32] L. Wilson, R.S.J. Sparks, G.P.L. Walker, Explosive volcanic eruptions–IV. The control of magma properties and conduit geometry on eruption column behavior, Geophys. J. Astron. Soc. 63 (1980) 117–748.
[33] C. Klug, K.V. Cashman, Vesiculation of May 18, 1980, Mount St. Helens magma, Geology 22 (1994) 468–472.
[34] K.V. Cashman, M.T. Mangan, Physical aspects of magmatic degassing II. Constrains on vesiculation processes from textural studies of eruptive products, Rev. Mineral. 30 (1994) 447–478.
[35] R.S.J. Sparks, S. Brazier, New evidence for degassing processes during explosive eruptions, Nature 295 (1982) 218–220.
[36] J.C. Eichelberger, C.R. Carrigan, H.R. Westrich, R.H. Price, Non-explosive silicic volcanism, Nature 323 (1986) 598–602.
[37] J.H. Fink, S.W. Anderson, C.R. Manley, Textural constraints on effusive silicic volcanism: beyond the permeable foam model, J. Geophys. Res. 97 (1992) 9073–9083.
[38] S.W. Anderson, J.H. Fink, The development and distribution of surface textures at the Mount St. Helens dome, in: J.H. Fink (Ed.), Lava Flows and Domes, Springer, Berlin, 1990, pp. 25–46.
[39] D.A. Swanson, R.T. Holcomb, Regularities in growth of the Mount St. Helens dacite dome 1980–1986, in: J.H. Fink (ed.), Lava Flows and Domes, Springer, Berlin, 1990, pp. 3–24.
[40] K.V. Cashman, J.E. Taggart, Petrologic monitoring of 1981 and 1982 eruptive products from Mount St Helens, Science 221 (1983) 1385–1387.
[41] M.B. Epel'baum, I.V. Babashov, T.P. Salova, Surface tension of felsic magmatic melys at high temperatures and pressures, Geokhimya 3 (1973) 461–464.
[42] M. Alidibirov, D.B. Dingwell, Magma fragmentation by rapid decompression, Nature 380 (1996) 146–148.
[43] J.E. Gardner, R.M.E. Thomas, C. Jaupart, S. Tait, Fragmentation of magma during Plinian volcanic eruptions, Bull. Volcanol. 58 (1996) 144–162.